

## Effect of magnetic stirring on AlFeSi intermetallics of an A356 aluminum alloy

Óscar Bustos<sup>1</sup>, Ricardo Leiva<sup>1</sup>, Christian Sánchez<sup>1</sup>

<sup>1</sup>Universidad de Santiago de Chile, Facultad de Ingeniería, Departamento de Ingeniería Metalúrgica. Av. Lib. Bernardo O'Higgins 3363, Santiago, Chile.

e-mail: oscar.bustos@usach.cl, ricardo.leiva.i@usach.cl, christian.sanchez@usach.cl

### ABSTRACT

The effect of the application of forced convection during the continuous solidification of A356 aluminum alloy over microstructural parameters of AlFeSi phases has been presented in this work. The investigation has been made on the fact that as an alloy solidifies under the action of a rotating magnetic field; a non-dendritic casting structure will be obtained. The Al-Si alloy has been studied using magnetic stirring equipment with permanent magnets. This device has allowed the study of the rotational speed (degree of stirring) effect on the micro- and macro- solidification structure. Different analyses and tests have been carried out, such as micro- and macro-structural analysis. The results have shown that magnetic stirring affects the cooling curves, expanding the solidification range.

Microstructural evolution of the alloys has also been observed, from a 100% dendritic structure to a mature rosette type structure, in addition to a notable grain size decrease, which may improve the material's mechanical behavior. The results show that all the microstructural parameters of the AlFeSi phases (quantity, size, shape factor, particle area, and aspect ratio) decrease when stirring is applied to the alloy during its solidification.

**Keywords:** Grain refinement; Forced convection; Solidification; AlFeSi.

### 1. INTRODUCTION

It is known that aluminum and its alloys make up more than 80% of the production of nonferrous alloys. Therefore, it is necessary to find methods that allow getting casting materials which offer the best possible performance, and in this search, technologies have been adapted for this purpose. Getting parts by casting alloys directly in a mold is, in general, an advantageous process when dealing with complex shape parts that are meant to be mass-produced, or very large parts. However, these products have a typical solidification structure that sometimes decreases their mechanical performance. Casters must deal with segregation [1–2], porosity caused by shrinkage during the solidification [1], and gas entrapment [3]. In order to deal with these problems and obtain pieces with good mechanical service, there has been developed methods like stirring the melt during the solidification (semisolid state) [4–5] or the addition of some alloying elements to modify the shape, size, and distribution of the phases in microstructure.

#### 1.1. Magnetic stirring

The use of magnetic fields during the solidification of metals dates back to the 1930s (their advantage is the lack of contact between the stirrer and the liquid metal). Magnetic stirring takes place due to the Lorentz force generated by an alternating inductor [6–8]. The magnetic stirrer is designed deliberately to produce convection in the liquid near the solidification front, through the application of low frequency magnetic fields to allow the Lorentz force acts deeply in the liquid metal. Two types of electromagnetic stirrers are commonly used: the linear stirrer and the rotatory stirrer. A linear stirrer operates as an induction furnace. This consists of a battery of coils around the molten metal to create a primary motion that recirculates in the melting direction. A rotary stirrer is an electric motor, which uses a rotary magnetic field to produce a spiral motion in the liquid. These types of stirring can be applied individually or combined, and the stirring can be applied in different stages of the solidification.

The effect of the stirring over the microstructure (decrease of micro and macro segregation), mechanical properties and favoring of the shaping and/or mechanizing processes has been studied for various materials [9–14].

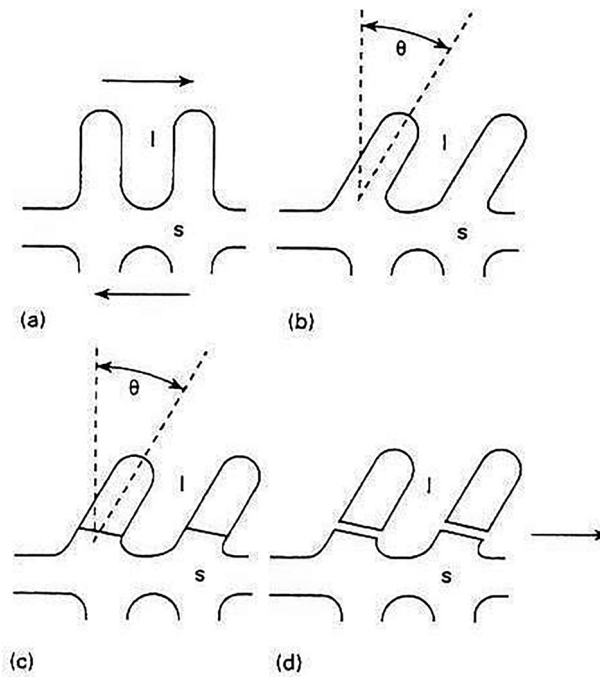


**Figure 1:** Dendritic fragmentation under forced convection [7].

This improvement, which is associated with the refining of the casting structure, is due to the dendritic fragmentation produced by the shearing stress caused by the liquid's convection ahead of the solidification front promoted by the magnetic stirring. However, there still is no full agreement as to how dendritic fragmentation takes place.

There are several theories that try to explain dendritic fragmentation, among them those proposed by Flemings in 1991 [6], which include fragmentation of the base of the dendritic branches caused by the high shear stress produced by magnetic stirring or by the re-melting of the dendritic roots of the branches, caused by dendritic ripening. Vogel et al. [7] propose a dendritic fragmentation mechanism that involves bending (caused by the shear stress) of the dendritic branches, giving rise to oriented dislocations forming a sort of low angle grain limit, which after bending more than 20 degrees is replaced by a liquid line (energetically more favorable), fracturing the dendrite as shown in Figure 1.

Finally, using an ultrasonic cavitation technique [15], it has been seen that the typical dendritic fragmentation mechanisms occur by fatigue, collapse, or fracture by bending, validating the first postulate of Flemings and that of Vogel et al., including fatigue as responsible for this phenomenon.

The fragments separated from the dendrites initially do not have a spherical shape, and under the proper conditions, they can be the site of new growth with a dendrite shape. In general, the structure of alloys subjected to processes in semisolid state (magnetic stirring) may be modified, evolving from a dendritic one to rosettes that still contain liquid trapped between its arms, and eventually spherical particles, as shown in the sequence of Figure 2.

## 1.2. Microstructure

Hypoeutectic Al-Si alloys as A356, once solidified, have basically two micro-constituents: one with low hardness and ductile, primary  $\alpha$ -Al solid solution, and an eutectic that consists of  $\alpha$ -Al and Si needles (with high hardness and fragile), where the  $\alpha$ -Al acts as a matrix for the Si phase. This eutectic has the particularity of being irregular, because it incorporates the characteristics of the solid solution high in aluminum and Silicon, which is practically insoluble, so its mechanical behavior is directly related to the shape, size, and distribution of Si [16–18].

### 1.2.1. Effect of iron in Al-Si alloys

Iron is always present in commercial cast aluminum alloys. The origin of iron is the use of steel tools in melting and casting operations and the use of scrap containing iron and rust. The presence of iron is detrimental for most cast aluminum alloys, and efforts are made to keep its levels as low as possible. However, in the case of

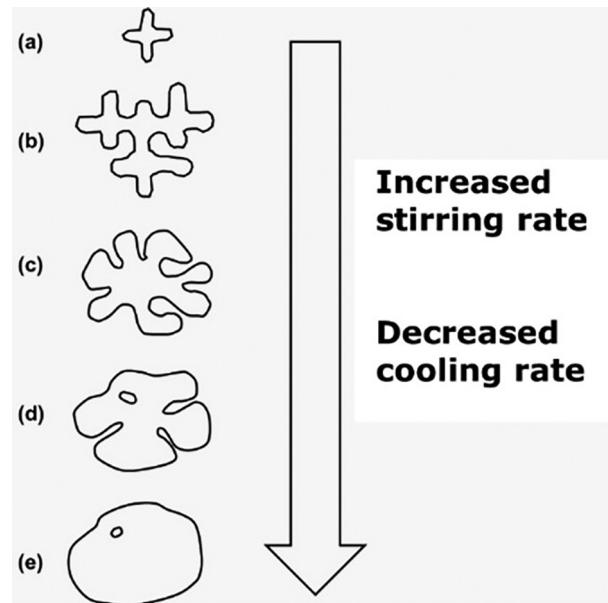


**Figure 2:** Time evolution of the structure in the semisolid state.

injection aluminum alloys, it is intentionally added to prevent adhesion to the shells. The formation of several iron-containing phases occurs and the effect of iron depends largely on the type and morphology of the phases it forms [19].

### 1.2.2. The types and morphologies of the iron phases

In an Al-Fe binary system, the equilibrium solid solubility of iron in aluminum is in the order of 0.03–0.05% at eutectic temperature (655 °C) and much lower at room temperature. The equilibrium phase with aluminum is usually designated FeAl<sub>3</sub> (40,7% Fe). In the Al-Fe-Si System, several ternary phases can be found in equilibrium: Fe<sub>2</sub>SiAl<sub>8</sub> (α), FeSiAl<sub>5</sub> (β), FeSi<sub>2</sub>Al<sub>4</sub> (δ) in high silicon alloys and FeSiAl<sub>3</sub> (γ). More ternary phases can be formed with higher amounts of iron and silicon. The invariant reactions of the corner rich in aluminum of the Al-Fe-Si system are shown in Table 1 [19].

For most commercial alloys, due to non-equilibrium solidification conditions, it is possible to find alloys in which FeAl<sub>6</sub>, FeAl<sub>3</sub>, Fe<sub>2</sub>SiAl<sub>8</sub>, FeSiAl<sub>5</sub> and FeSi<sub>2</sub>Al<sub>4</sub> coexist with each other and with silicon. High cooling rates tend to drive the eutectics to higher iron content and to disperse the FeSiAl<sub>5</sub> crystals.

The size and morphology of the iron phases in aluminum casting alloys depend on the composition of the alloy and the solidification conditions [20–24]. In commercial alloys, the iron phases can appear as Chinese script, needles, plates, or angular globules and in some circumstances, they can appear as petal-like particles. The size of the particles generally becomes smaller with increasing speed and cooling. Occasionally, especially in low-silicon alloys, FeSiAl<sub>5</sub> can have the morphology of Chinese script like needles (plates). Therefore, the identification of these phases only by means of their morphology may be misleading. It is usually associated to Chinese script with Fe<sub>2</sub>SiAl<sub>8</sub> (α) and to the shape of needles to the FeSiAl<sub>5</sub> (β) phase.

The effect of iron on the mechanical properties of alloys is related to the type and morphology of the compounds it forms, as well as their quantity. In general, the intermetallic phases of iron increase hardness and decrease ductility. The compounds are essentially insoluble and may be responsible for the increase in strength,

**Table 1:** Reactions during the solidification of the A356 (quaternary) alloy.

Reaction number	Reaction	Temperature
1 (primary)	Development of the Al primary phase	614 °C
2 a (post dendritic)	Liq→Al+Al <sub>13</sub> Fe <sub>3</sub> Mn <sub>3</sub> Si <sub>2</sub> (α)	594°C
2 b	Liq→Al+Al <sub>5</sub> FeSi (β)+ Al <sub>13</sub> Fe <sub>3</sub> Mn <sub>3</sub> Si <sub>2</sub> (α)	594°C
3 a (eutectic)	Liq→Al+Si+Al <sub>5</sub> FeSi (β)	572 °C
4 (post eutectic)	Liq→Al+Si+Mg <sub>2</sub> Si(β')	555°C

particularly at high temperatures. Chinese script type morphs are preferred due to their lesser effect on loss of toughness compared to acicular morphs.

## 2. EXPERIMENTAL PROCEDURE

The raw material used in the experiments is an A356 aluminum-silicon-magnesium alloy. The chemical composition is presented in Table 2.

The A356 alloy studied was solidified under different degrees of magnetic stirring, for which the samples were cast in a crucible placed over a magnetic stirring apparatus (Figure 3a) which consists of:

- A cylindrical frame, in which there are three pairs of permanent magnets equidistant from one another (Figure 3b).
- Coupling components to an alternating current motor.
- A 120 mm long and 50 mm outer diameter crucible made of AISI 316L stainless steel. The tube is lined on the inside with high alumina refractory concrete that shapes the crucible's cavity (Figure 3c).

The equipment can have three different rotational speeds (650 rpm, 980 rpm, and 1540 rpm). The alloy was first melted in a crucible whose frame did not turn, providing the sample designated with subscript 0. After it solidified, the same procedure was followed to provide the samples with subscripts 1, 2, and 3, corresponding to frame turning speeds of 650 rpm, 980 rpm, and 1540 rpm, respectively, Table 3.

**Table 2:** Chemical composition of the alloy used.

Alloy	%Si	%Fe	%Mg	%Al
A	7.00	0.10	0.25	Balance

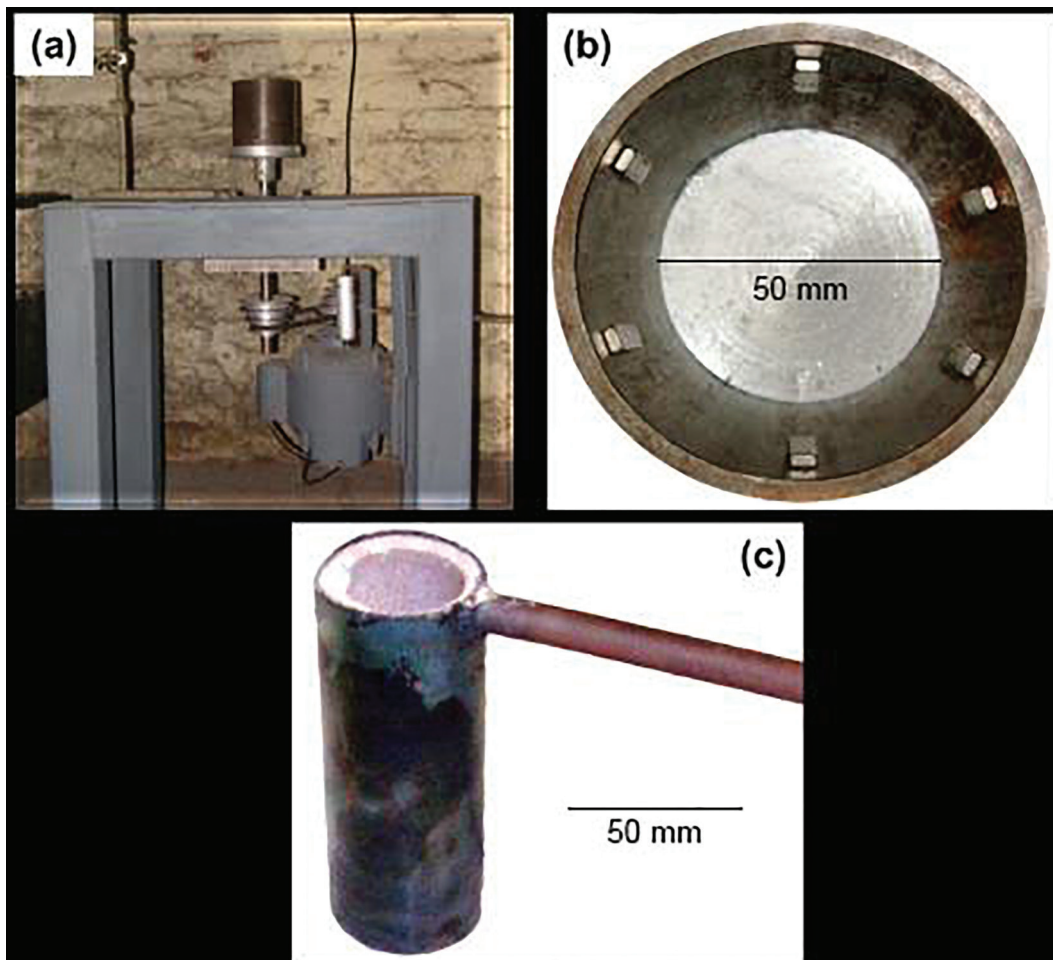


**Figure 3:** Equipment and materials used. (a) Magnetic stirring equipment; (b) turning frame ; (c) crucible.

**Table 3:** Sample identification.

Turning speed (rpm)	Sample
0	A <sub>0</sub>
650	A <sub>1</sub>
980	A <sub>2</sub>
1540	A <sub>3</sub>

Once solidified, the samples were cut longitudinally with a cooled abrasive cutting disc. Then, they were prepared for the macrographic analysis to reveal their casting structure, etching them with Poulton's reagent. After getting their structures, the samples were prepared for metallographic analysis according to ASTM E3-17 [25], and then they were etched with 0.5% HF, revealing their microstructure. Finally, the AlFeSi-type intermetallic compounds ( $\alpha$  and  $\beta$ ) were characterized with the help of a Philips scanning electron microscope (SEM), model XL-30, owned by the Center for Technical Studies and Research in Guipúzcoa, CEIT, San Sebastian, Spain, and its chemical analysis using a microprobe (X-ray dispersive energy, EDAX) set to an accelerating voltage of 20KV to ensure that the electron-sample interaction involves only one phase.

For the characterization of the AlFeSi phases, specimens were observed by optical microscopy and SEM. The criteria applied to discriminate between alpha and beta phases in particle recognition were as follows [24]:

- Particle morphology: since the beta phase has an acicular or plate-like appearance, and the alpha phase has a "Chinese script" or globular appearance. Therefore, the beta phase will have a high aspect ratio and shape factor. Where the aspect ratio is defined as:

$$AR = \frac{d_{\max}}{d_{\min}} \quad (1)$$

Where  $d_{\max}$  is the largest diameter and  $d_{\min}$  is the smallest diameter.

And the shape factor is defined as

$$SF = \frac{p^2}{4\pi A} \quad (2)$$

Where P is the perimeter and A is the area of the particle.

- Color (optical microscopy): Given that in optical microscopy for specimens etched with 0.5% HF, the beta phase is dark gray, while the alpha phase has a light gray color, with variable shades tending to light brown depending on the content of substitutional solutes such as Mn, Cr and Cu present in it.
- Light intensity (SEM, backscattering): The alpha phase is bright, and the beta phase is opaque in SEM.
- Fe/Si ratio (measured by EDAX): Since the beta phase presents a ratio close to 1, the alpha phase, on the other hand, presents a ratio close to 2, although much higher ratios for the alpha phase have been reported in the literature [24]:
- Presence of substitutional solutes (measured by EDAX): since Mn, Cr and Cu go into solution in the alpha phase and not in the beta phase.

For a clear and accurate discrimination of particle types, the parameters in Table 4 were set to aid in identification

**Table 4:** Parameters used in the discrimination of AlFeSi particles.

Minimum Shape Factor, SF min	1.5
Maximum Shape Factor, SF max	15
Fe/Si max	1.75
Fe/Si min	1.25

Then, the procedure used was as follows:

- i. Observe morphology, color and evaluate shape factor.  
If the color agrees with those previously indicated, and  
If  $SF \leq SF_{min}$ , then the particle is alpha.  
Or if  $SF > SF_{max}$ , then the particle is beta.  
If not,
- ii. Measure Fe/Si Ratio (when possible)  
If  $Fe/Si \leq (Fe/Si)_{min}$  then the particle is beta.  
If  $Fe/Si > (Fe/Si)_{max}$  then Particle is alpha.

In case the Fe/Si ratio is between 1.25 and 1.75 it is not possible to discriminate with certainty the type of particle and therefore additional criteria must be used.

### 3. RESULTS AND DISCUSSION

#### 3.1. Macrographic analysis

Figure 4, present images related to macrographic analysis of the samples at different stirring speeds. The modification of the cast columnar structure and a marked decrease in the grain size are observed with the naked eye. The agitation generates shear stresses in the fluid that eventually cause fragmentation of the growing dendritic branches.

Figure 5 shows that as the degree of stirring increases, a smaller grain size is obtained from the linear intersection described in the ASTM E112–13 standard [26]. In the absence of stirring, it was also seen that there is a tendency to develop a columnar dendritic structure, which tends to structures close to equiaxiality as the stirring speed increases.

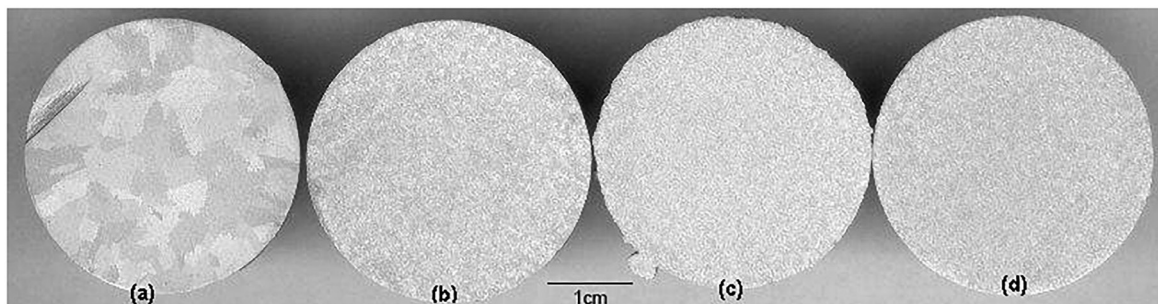


Figure 4: Macrographs of the samples. (a) no stirring; (b) 650 RPM stirring; (c) 980 RPM stirring; (d) 1540 RPM stirring.

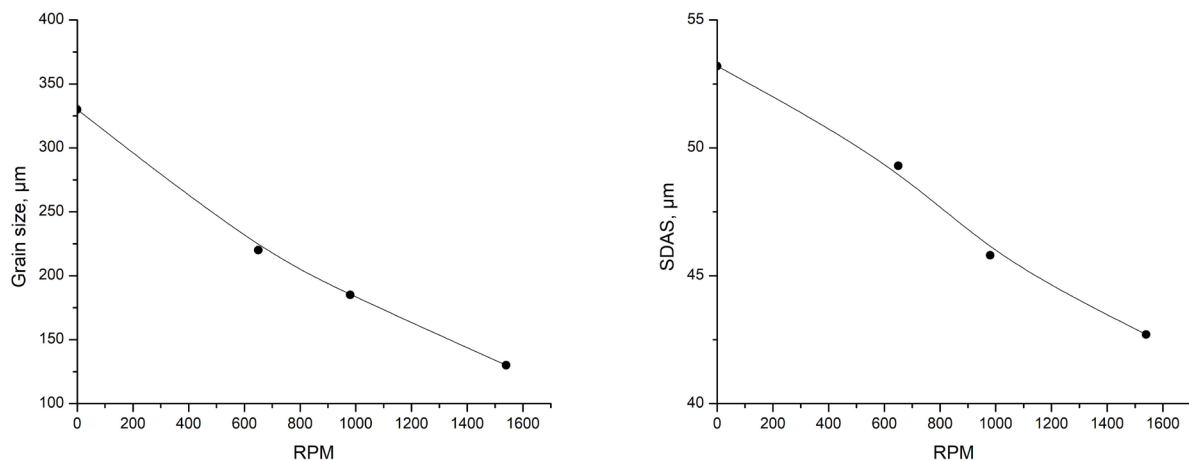


Figure 5: Grain sizes and SDAS of the samples.

The secondary dendritic arms spacing (SDAS) decreases as the stirring speed increases. This can be explained by magnetic stirring. The solute accumulated in the liquid in front of the solid / liquid interface will be removed by the convective flow resulting in a higher solute gradient and greater constitutional supercooling, this causes a marked reduction in SDAS relative to the solidified structure without stirring (for lowest stirring speed), Figure 5. As solidification proceeds, the number of dendritic branches that will be fragmented by increasing interaction between them. The dendritic fragments that have been initially separated are not spheroidal and if conditions are favorable, they will continue to grow as dendrites. However, ripening processes obtained for the reduction of the surface area will operate and the regions of high curvature will be eliminated or reduced by diffusion of solute in the liquid. Ripening can be accelerated by increasing stirring since this increases solute transport [18].

Higher stirring speeds promote a change in morphology from dendritic to ripened rosettes containing liquid between the branches, increasing SDAS as described by Flemings [6] and illustrated in Figure 2.

The modification of the solidification structure is related to the transport of solute and the presence of shear stresses in the fluid that augments by increasing the speed of rotation of the magnetic field, product of Lorentz forces. Note, furthermore, that the microstructures presented in Figure 7 (b), (c) and (d) show a decreasing agglomerate size distribution, which eventually responds to an increase in the solute gradient at the solid-liquid interface during solidification, which expands constitutional supercooling and consequently dendritic growth. The increase in constitutional supercooling is confirmed by analyzing the cooling curves in Figure 6, from which it can be deduced that the application of a rotating magnetic field that produces agitation of the melt significantly shifts the eutectic transformation towards lower temperatures, which results in microstructural refinement.

### 3.2. Micrographic analysis

The Figure 7 shows the typical microstructure of these alloys, which consists of an  $\alpha$ -Al matrix (clear phase), with the presence of eutectic (dark constituent), in agreement with what was described in section 1.

#### 3.2.1. Analysis of intermetallic compounds particles

The images in Figure 8 show the phases that compose the microstructure of the A356 alloy without agitation, in it can be observed particles with different contrast, particles 1, 6 and 7 as  $\alpha$ AlFeSi, presenting the highest contrast and Chinese script morphology. This is confirmed by the analyses obtained by EDAX in Table 5, where the presence of substitutional solutes and a Fe/Si ratio higher than 1.5 can be observed.

Particles 4, 5 and 8, with a lower degree of contrast, can be identified as  $\beta$ AlFeSi, presenting an acicular morphology with a high aspect ratio, absence of substituent solutes and low Fe/Si ratio.

In addition, particles of lower contrast with an acicular morphology are observed which corresponding to eutectic silicon, EDAX 3, and the background of greater opacity corresponds to the primary phase rich in aluminum, EDAX 2.

With the results of the phase identification of the as cast samples with no stirring, it is possible to identify phases for all experimental conditions, these results are shown in Figures 9 to 11 and Tables 6 to 8.

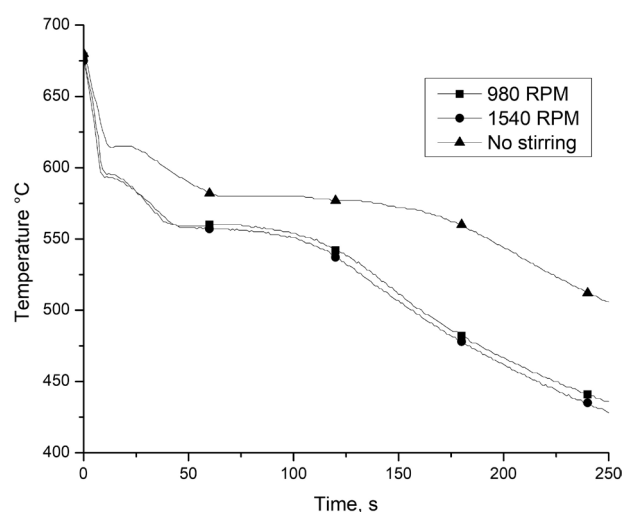
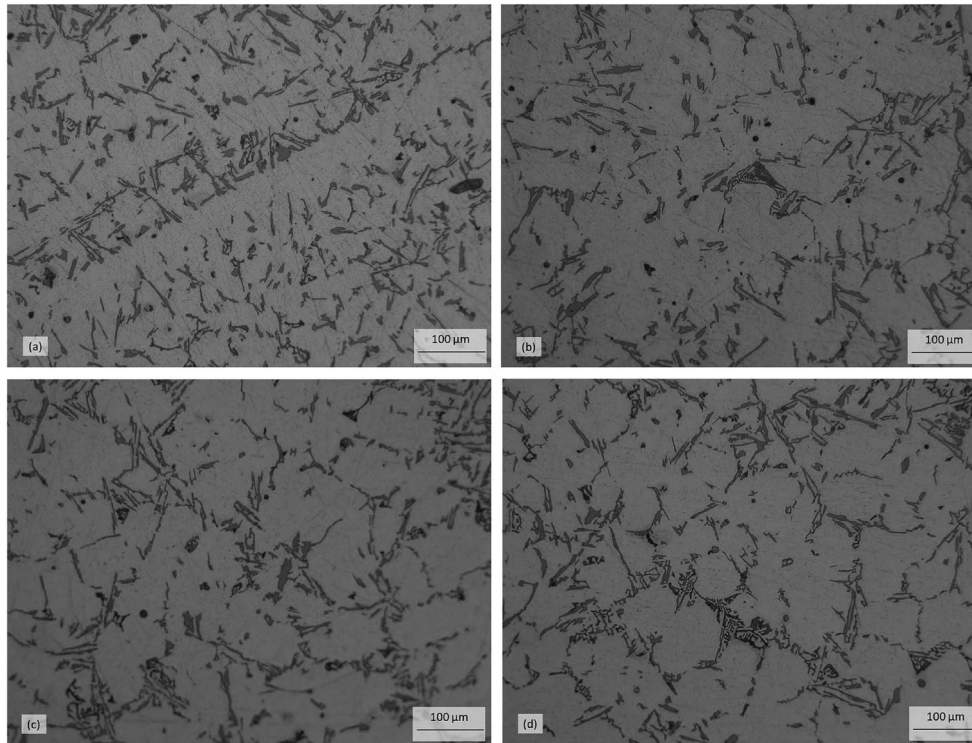


Figure 6: Cooling curves obtained at different stirring conditions.



**Figure 7:** Micrographs of the A356 alloy, (a) no stirring; (b) 650 RPM stirring; (c) 980 RPM stirring; (d) 1540 RPM stirring.

These two phases,  $\beta\text{AlFeSi}$  ( $\text{FeSiAl}_3$ ) and  $\alpha\text{AlFeSi}$  ( $\text{Fe}_2\text{AlSi}_8$ ), can be found in equilibrium with aluminum. Another phase may be present in high silicon alloys,  $\text{FeSi}_2\text{Al}_4$  ( $\delta$ ) and a fourth phase,  $\text{FeSiAl}_3$  ( $\gamma$ ), will be formed in high iron and silicon alloys. Evidence indicates that equilibrium is not reached in this system under commercial solidification conditions and elements such as chromium and manganese are added to stabilize it [19].

The ranges of existence of the ternary phases in the solid state are very far from their range of primary crystallization, and to establish the equilibrium, it is necessary to complete the peritectic reactions. For this reason, most commercial alloys are not in equilibrium and it is common to find alloys in which all the mentioned phases can coexist with each other and with silicon. In alloys with heat treatment, equilibrium can be reached by solid state diffusion and the  $\text{FeSiAl}_3$  ( $\beta$ ) phase can be found with Chinese script morphology, characteristic of  $\text{Fe}_2\text{SiAl}_8$  ( $\alpha$ ).

A variety of intermetallic phases can be formed, such as:  $\text{FeAl}_3$ ,  $\alpha\text{AlFeSi}$ ,  $\beta\text{AlFeSi}$ .

In a quaternary system these reactions can occur over a range of temperatures. Whatever the actual solidification conditions are, the peritectic reactions by depending on diffusion mechanisms will be suppressed (at high cooling rates) and the remaining liquid will proceed to react to the next available eutectic. Thus a solidification sequence could be [24]:

1. Primary dendrites
2.  $\text{L} \rightarrow \text{Al} + \text{FeAl}_3$
3.  $\text{L} + \text{FeAl}_3 \rightarrow \text{Al} + \alpha\text{AlFeSi}$  (suppressed)
4.  $\text{L} \rightarrow \text{Al} + \alpha\text{AlFeSi}$
5.  $\text{L} + \alpha\text{AlFeSi} \rightarrow \text{Al} + \beta\text{AlFeSi}$  (suppressed)
6.  $\text{L} \rightarrow \text{Al} + \beta\text{AlFeSi}$
7.  $\text{L} \rightarrow \text{Al} + \beta\text{AlFeSi} + \text{Si}$

Once the particles have been characterized, the images can be analyzed with Image Pro Plus 6.0 software, quantifying the morphological parameters of shape factor and aspect ratio, together with the identification of their color and contrast to size the total amount of  $\text{AlFeSi}$  phases and discriminate between  $\alpha\text{AlFeSi}$  and  $\beta\text{AlFeSi}$  for different processing conditions, as shown in Figure 12. Furthermore, the relative amount of the  $\alpha\text{AlFeSi}$  phase is similar to that of the  $\beta\text{AlFeSi}$  phase in the unstirred condition. In contrast, when the melt is stirred at 1450 RPM during solidification the amount of resulting  $\alpha\text{AlFeSi}$  is almost twice that of  $\beta\text{AlFeSi}$  for the stirred condition.

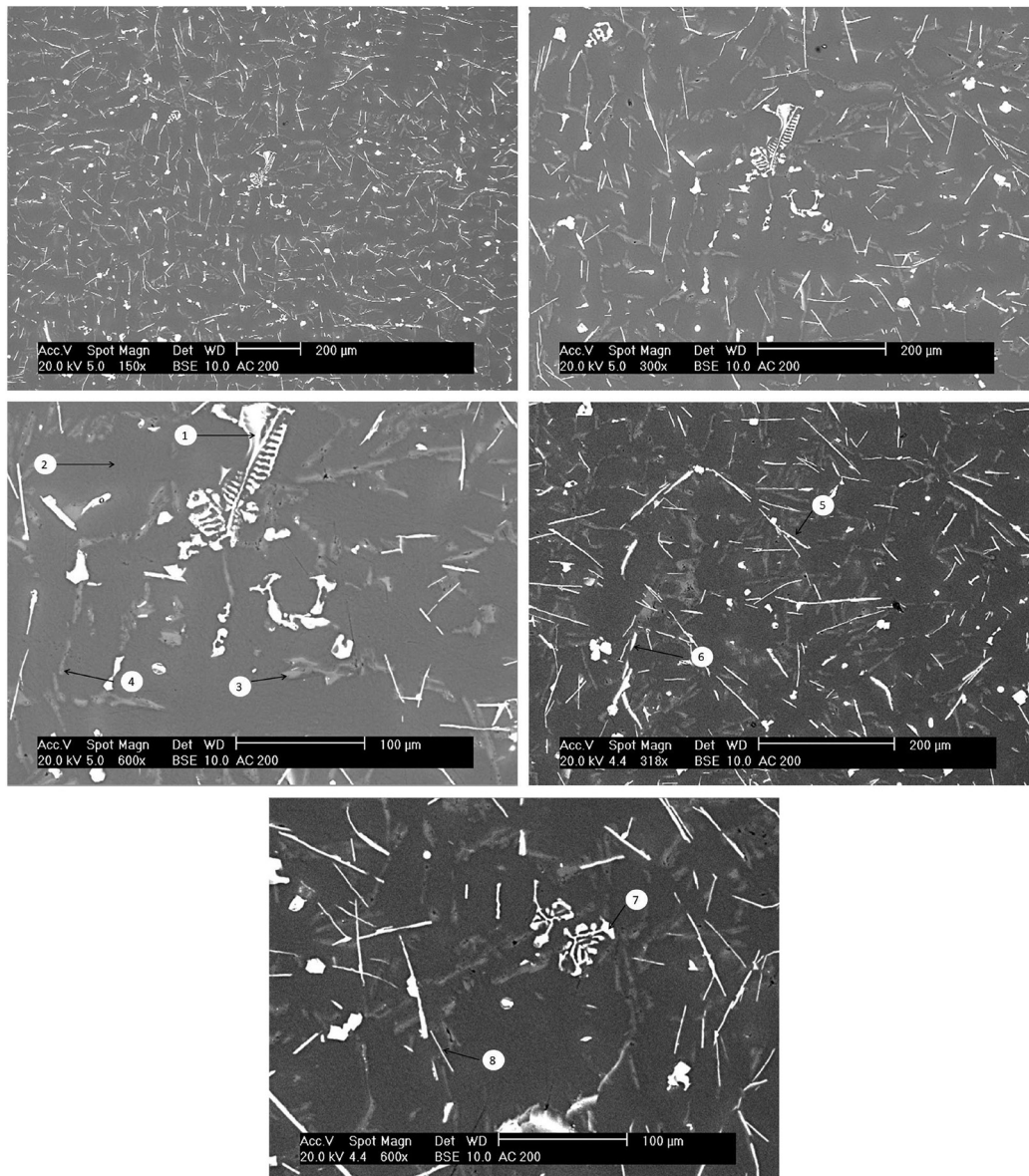


**Figure 8:** SEM images of the sample in mold casting condition at 200 ° C.

**Table 5:** EDAX analysis of sample particles without stirring.

Sample A0, no stirring		% atomic								
Particle number	Type	Mg	Al	Si	Ag	Cr	Mn	Fe	Ni	Fe/Si
1	$\alpha$ AlFeSi	2.22	71.37	8.99	0.39	2.76	0.89	13.62	0.31	1.51
2	Primary Al	3.19	93.49	1.2	2.09	–	–	–	–	–
3	Silicon	1.4	2.2	77.4	–	–	–	–	–	–
4	$\beta$ AlFeSi	2.2	71.6	18.0	0.6	–	0.2	7.4	–	0.41
5	$\beta$ AlFeSi	1.7	47.89	44.2	0.22	–	0.24	5.63	0.17	0.13
6	$\alpha$ AlFeSi	2.23	68.13	9.8	0.27	5.19	1.19	12.94	0.26	1.32
7	$\alpha$ AlFeSi	2.27	68.45	9.75	0.3	5.9	1.07	12.1	0.17	1.24
8	$\beta$ AlFeSi	1.81	55.82	37.2	0.3	–	0.19	4.52	0.11	0.12

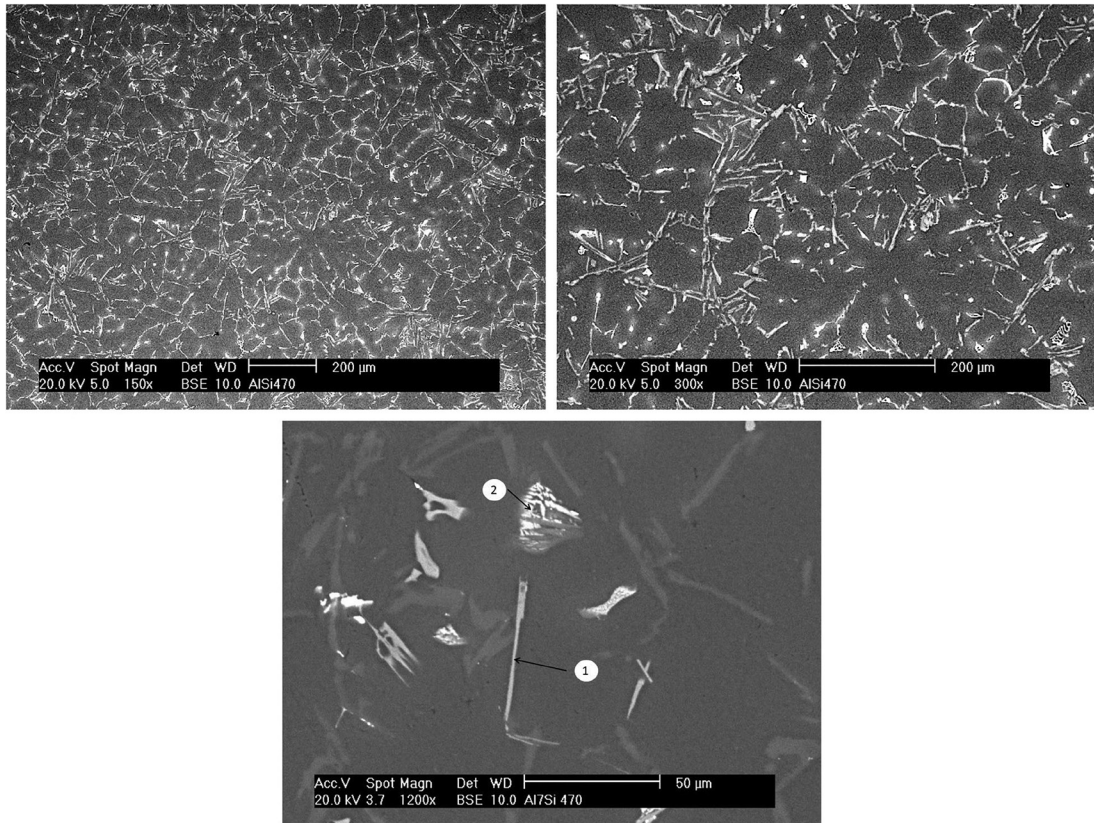


Figure 9: SEM images of the sample in stirred condition at 650 RPM.

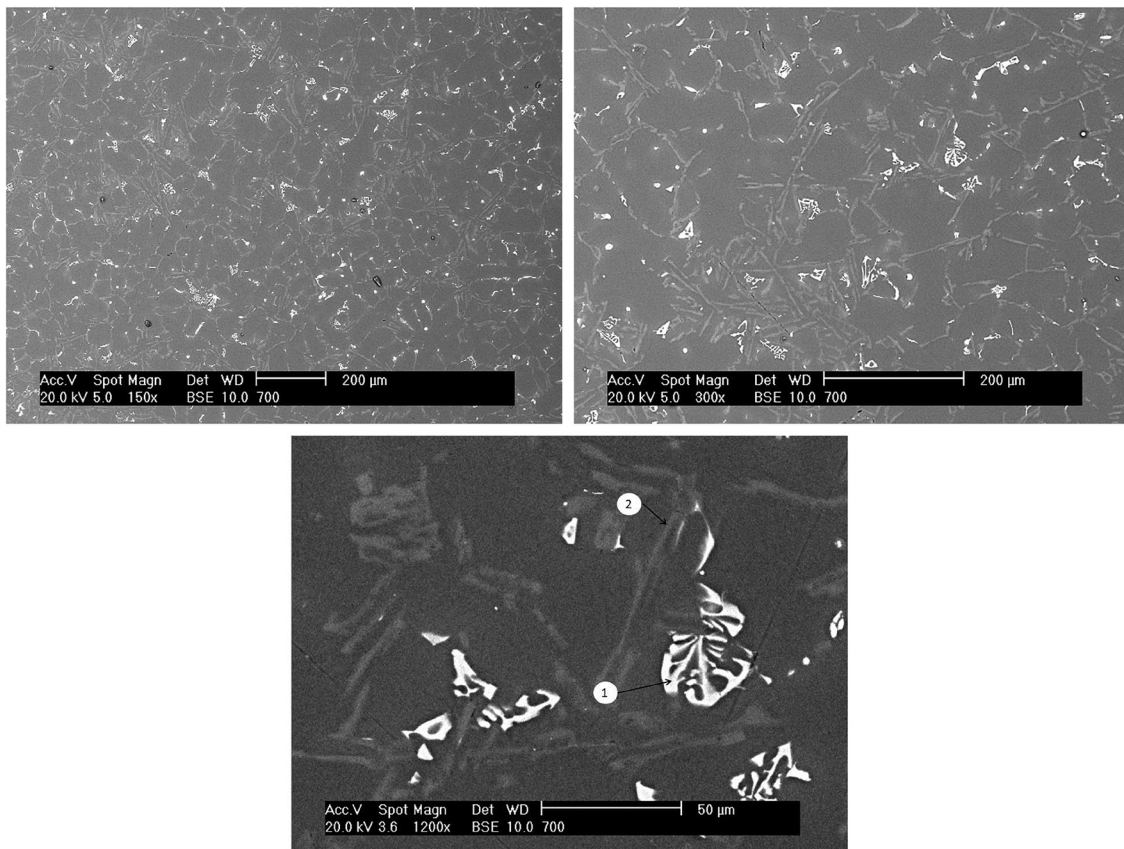


Figure 10: SEM images of the sample in stirred condition at 980 RPM.

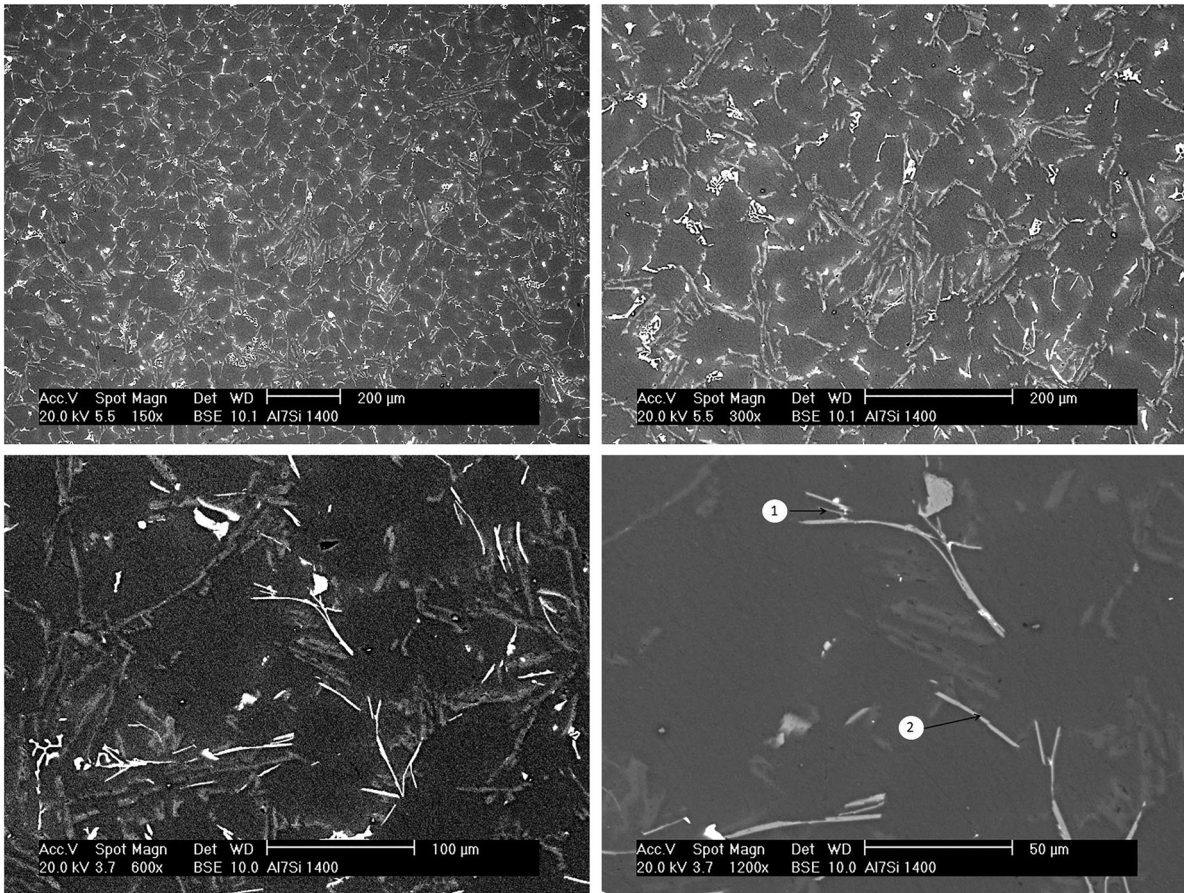


Figure 11: SEM images of the sample in stirred condition at 1540 RPM.

Table 6: EDAX analysis of particles in stirred condition at 650 RPM.

Sample A1, stirring at 650 RPM		% atomic						
Particle number	Type	Mg	Al	Si	Mn	Fe	Cu	Fe/Si
1	$\beta$ AlFeSi	0	75.1	13.0	0	11.9	0	1.4
2	$\alpha$ AlFeSi	2.01	89.5	2.7	0.42	3.12	2.25	1.77

Table 7: EDAX analysis of particles in stirred condition at 980 RPM.

Sample A2, stirring at 980 RPM		% atomic					
Particle number	Type	Si	Cr	Mn	Fe	Cu	Fe/Si
1	$\alpha$ AlFeSi	34,21	2,09	4,46	49,91	9,33	1,46
2	$\beta$ AlFeSi	23.44			62.16		1.64

Table 8: EDAX analysis of particles in stirred condition at 1540 RPM.

Sample A1, stirring at 1540 RPM		% atomic					
Particle number	Type	Si	Cr	Mn	Fe	Cu	Fe/Si
1	$\alpha$ AlFeSi	8.19	1.24	0.97	12.32	0.93	1.5
2	$\beta$ AlFeSi	89.26			10.74		0.12

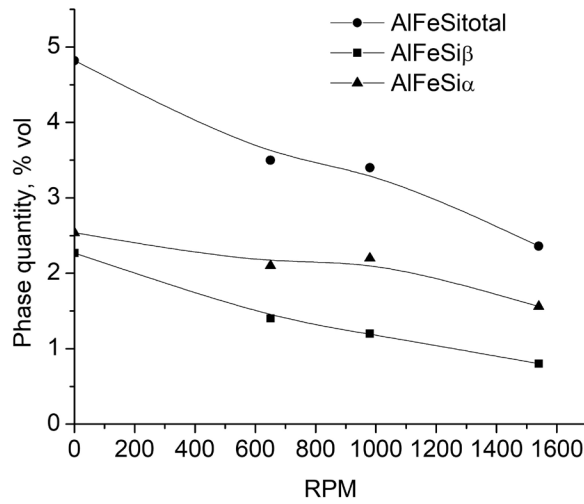


Figure 12: Quantity of AlFeSi phases.

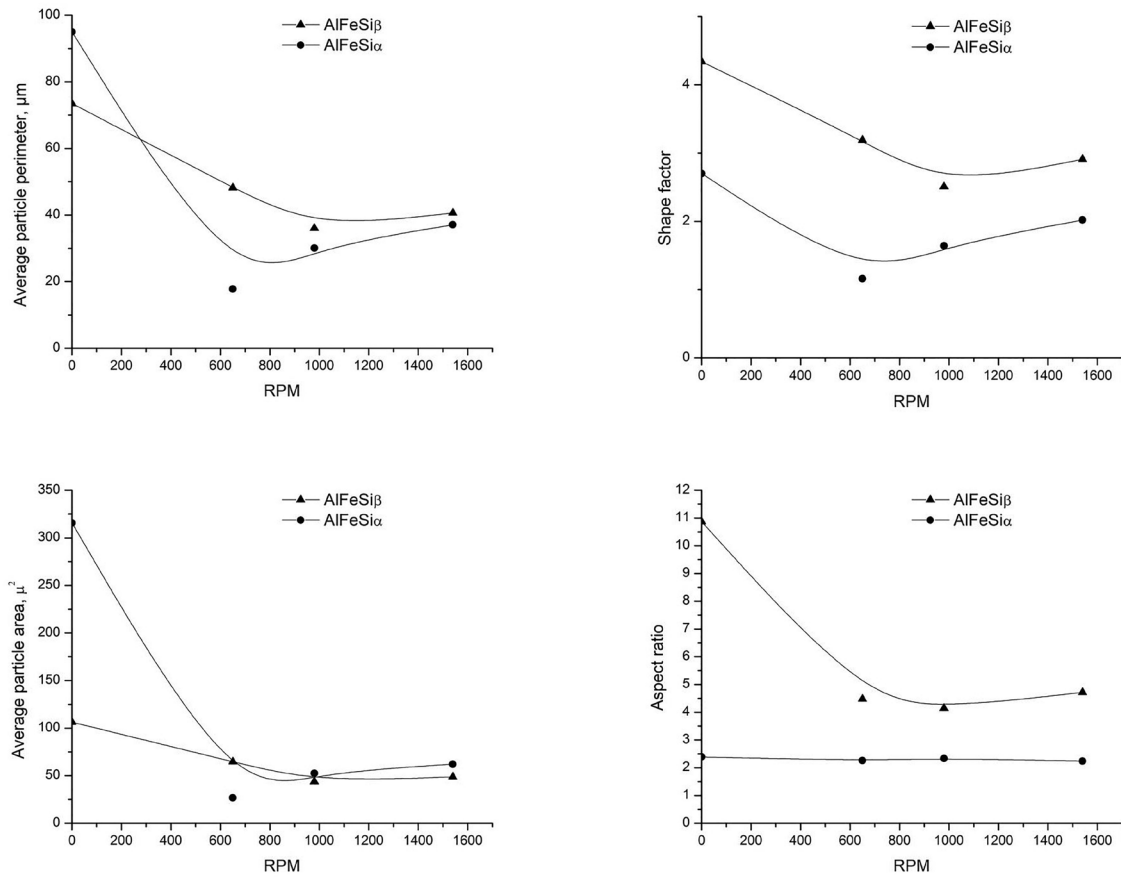


Figure 13: Microstructural parameters of the AlFeSi phases.

This is due to the higher solidification rate which inhibits the peritectic transformations involved in the formation of  $\beta$ AlFeSi, which in turn generates a higher microstructural refinement and lower amount of intermetallic phases.

The effect of applying stirring to the melt during solidification on the morphological characteristics of the AlFeSi compounds is shown in Figure 13, where a decrease in size can be observed, especially of the  $\alpha$ AlFeSi compounds, confirms the microstructural refining. A decrease in the form factor of both types of particles is observed, so that less acicular phases will be obtained and finally, the aspect ratio of the phase  $\beta$ AlFeSi confirms the observed microstructural refining, being able to observe a relationship between the spacing between dendritic arms, SDAS, and the size of the intermetallic phases, if the SDAS decreases, as seen in Figure 5, the intermetallic phases cannot agglomerate and grow in size.

#### 4. CONCLUSIONS

1. The agitation of the liquid bath by means of the application of magnetic fields causes a reduction of the average dendritic grain size and the secondary dendritic spacing, evolving from an equiaxed dendrite morphology to a rosette. This morphology is consistent with the cooling conditions and thermal gradient during solidification in the magnetic stirring equipment.
2. The increase in constitutional supercooling is ratified when analyzing the cooling curves, it follows from them that the application of a rotating magnetic field that produces agitation of the melt, significantly shifts the eutectic transformation towards lower temperatures, which translates into a refinement of the silicon phase and AlFeSi-type intermetallic phases.
3. The amount of total AlFeSi phases is much lower for the conditions where agitation has been applied. Furthermore, the relative amount of  $\alpha$ AlFeSi is similar to the amount of  $\beta$  AlFeSi phase in the non-stirred condition, when stirring the melt during solidification the amount of  $\alpha$  AlFeSi is almost double that of  $\beta$ AlFeSi for the stirred condition. with 1540 RPM, this, as in the primary phase, is related to the higher cooling speed and the shift of the transformation temperatures towards lower values, Figure 6, which means, on the one hand, into a microstructural refining and on the other hand in a smaller amount of intermetallic phases.

#### 5. ACKNOWLEDGEMENTS

The authors acknowledge the financial support for this research to DICYT USACH and the doctoral program in Materials Science and Engineering of USACH.

#### 6. BIBLIOGRAPHY

- [1] PORTER, D., EASTERLING K., SHERIF M., *Phase Transformations in Metals and Alloys*. 2 ed. Boca Ratón: CRC press, 2009.
- [2] SHEWMON, P., *Transformations in metals*. 1 ed. New York: McGraw-Hill, 1969.
- [3] BROWN, J., *Foseco non-ferrous foundryman's Handbook*. 1 ed. Oxford: Butterworth-Heinemann, 1999.
- [4] MOHAMMED, M., OMAR, M., SALLEH, M., *et al.*, "An overview of semi-solid metal processing", *Australian Journal of Basic and Applied Sciences*, v. 19, n. 8, pp. 369–373, 2014.
- [5] MOHAMMED, M., OMAR, M., SALLEH, M., *et al.*, "Semisolid metal processing techniques for non-dendritic feedstock production", *The Scientific World Journal*, v. 2013, n. 1, pp. 1–16, 2013.
- [6] FLEMINGS, M., "Behavior of metal alloys in the semisolid state", *Metallurgical transactions A*, v. 22, n. 5, pp. 957–981, 1991.
- [7] VOGEL, A., DOHERTY, R., "Proceedings of solidification and casting of metals conference", *Metals Society*, v. 192, n. 1, pp. 518–525, 1979.
- [8] BUSTOS, O., LEIVA, R., SÁNCHEZ, C., *et al.*, "Evolución microestructural y propiedades reológicas de la aleación AA6063 fabricada mediante técnicas de procesado semisólido (SIMA y MHD)", *Revista de metalurgia*, v. 43, n. 3, pp. 165–180, 2007.
- [9] AGRAWAL, S., GHOSE, A., CHAKRABARTY, I., "Effect of rotary electromagnetic stirring during solidification of In-situ Al-TiB 2 composites", *Materials & Design*, v. 113, n. 1, pp. 195–206, 2017.
- [10] WILLERS, B., ECKERT, S., NIKRITYUK, P., *et al.*, "Efficient melt stirring using pulse sequences of a rotating magnetic field: Part II. Application to solidification of Al-Si alloys", *Metallurgical and Materials Transactions B*, v. 39, n. 2, pp. 304–316, 2008.
- [11] NATORI, K., UTSUNOMIYA, H., TANAKA, T., "Improvement in formability of semi-solid cast hypoeutectic Al-Si alloys by equal-channel angular pressing", *Journal of Materials Processing Technology*, v. 240, n. 1, pp. 240–248, 2017.
- [12] WEI H., XIA F., QIAN S., *et al.*, "Effect of permanent magnetic stirring on the solidification microstructure and ingot quality of Al-Cu alloys", *Journal of Materials Processing Technology*, v. 240, n. 1, pp. 344–353, 2017.
- [13] KUMAR, S., SUMAN, K., RAVINDRA, K., *et al.*, "Microstructure, mechanical response and fractography of AZ91E/Al<sub>2</sub>O<sub>3</sub> (p) nano composite fabricated by semi solid stir casting method", *Journal of Magnesium and Alloys*, v. 5, n. 1, pp. 48–55, 2017.
- [14] ZIMMERMANN, G., PICKMANN, C., HAMACHER, M., *et al.*, "Fragmentation-driven grain refinement in directional solidification of AlCu10wt-% alloy at low pulling speeds", *Acta Materialia*, v. 126, n. 1, pp. 236–250, 2017.

- [15] WANG, F., TZANAKIS, I., ESKIN, D., *et al.*, “In situ observation of ultrasonic cavitation-induced fragmentation of the primary crystals formed in Al alloys”, *Ultrasonics Sonochemistry*, v. 39, n. 1, pp. 66–76, 2017.
- [16] JOSEPH, S., KUMAR, S., “Role of Si modification on the compressive flow behavior of Al–Si based alloy”, *Materials Characterization*, v. 110, n. 1, pp. 272–281, 2015.
- [17] HEGDE, S., PRABHU, K., “Modification of eutectic silicon in Al–Si alloys”, *Journal of materials science*, v. 43, n. 9, pp. 3009–3027, 2008.
- [18] BUSTOS, O., ALLENDE, R., LEIVA, R., *et al.*, “Effect of magnetic stirring, grain modification and refinement on the solidification structure of an A356 aluminum alloy”, *Matéria (Rio de J.)*, v. 26, n. 1, e12927, 2021.
- [19] MONDOLFO, L., “*Aluminum Alloys: Structure and properties*”, Oxford: Butterworth & co., 1976.
- [20] NILSEN, K.E., KOENIS, P.T.G., “Quantitative analysis of the homogenizing heat treatment by means of AlFeSi particle analysis and the effect on productivity”. In: *7th International Aluminum Extrusion Technology Seminar*, pp. 69–75, Chicago, 2000.
- [21] LEE, G., KIM, M., PARK, J., “Elimination of Iron in Molten Aluminum Scrap by Electromagnetic Stirring Technique”, In: *8° Pacific Rim International Congress on Advanced Materials and Processing*, Cham, 2013.
- [22] MIKOLAJCZAK, P., RATKE L., “Effect of stirring induced by rotating magnetic field on b-Al<sub>15</sub>FeSi intermetallic phases during directional solidification in AlSi alloys”, *International Journal of Cast Metals Research*, v. 26, n. 6, pp. 339–353, 2013.
- [23] ZHANG, Y., SVYNARENKO, K., ZOU, Q., *et al.*, “Effect of rotating magnetic field and manganese on the formation of iron-containing intermetallic compounds in Al-Si alloy”, In: *8th International Conference on Electromagnetic Processing of Materials*, Cannes, 2015.
- [24] ANDERSON, A., “Physical Metallurgy and extrusion of 6063 alloy”, In: *5° International Aluminum Extrusion Technology Seminar*, pp. 43–56, Chicago, 1984.
- [25] AMERICAN SOCIETY FOR TESTING AND MATERIALS (ASTM). *E3–11: Standard Guide for Preparation of Metallographic Specimens*. Pennsylvania: ASTM, 2017.
- [26] AMERICAN SOCIETY FOR TESTING AND MATERIALS (ASTM). *E112–13: Standard Test Methods for Determining Average Grain Size*, Pennsylvania: ASTM, 2013.